MetaAD: Metabolism-Aware Anomaly Detection for Parkinson's Disease in 3D ^{18}F-FDG PET

Haolin Huang[1†], Zhenrong Shen[2†], Jing Wang[3†], Xinyu Wang[1], Jiaying Lu[3], Huamei Lin[3], Jingjie Ge[3], Chuantao Zuo[3(✉)], and Qian Wang[1,4(✉)]

[1] School of Biomedical Engineering & State Key Laboratory of Advanced Medical Materials and Devices, ShanghaiTech University, Shanghai, China
qianwang@shanghaitech.edu.cn
[2] School of Biomedical Engineering, Shanghai Jiao Tong University, Shanghai, China
[3] Department of Nuclear Medicine/PET Center, Huashan Hospital, Fudan University, Shanghai, China zuochuantao@fudan.edu.cn
[4] Shanghai Clinical Research and Trial Center, Shanghai, China

Abstract. The dopamine transporter (DAT) imaging such as ^{11}C-CFT PET has shown significant superiority in diagnosing Parkinson's Disease (PD). However, most hospitals have no access to DAT imaging but instead turn to the commonly used ^{18}F-FDG PET, which may not show major abnormalities of PD at visual analysis and thus hinder the performance of computer-aided diagnosis (CAD). To tackle this challenge, we propose a Metabolism-aware Anomaly Detection (MetaAD) framework to highlight abnormal metabolism cues of PD in ^{18}F-FDG PET scans. MetaAD converts the input FDG image into a synthetic CFT image with healthy patterns, and then reconstructs the FDG image by a reversed modality mapping. The visual differences between the input and reconstructed images serve as indicators of PD metabolic anomalies. A dual-path training scheme is adopted to prompt the generators to learn an explicit normal data distribution via cyclic modality translation while enhancing their abilities to memorize healthy metabolic characteristics. The experiments reveal that MetaAD not only achieves superior performance in visual interpretability and anomaly detection for PD diagnosis, but also shows effectiveness in assisting supervised CAD methods. Our code is available at https://github.com/MedAIerHHL/MetaAD.

Keywords: Parkinson's disease · Brain PET · Unsupervised Anomaly Detection · Cross-modality Synthesis.

1 Introduction

Parkinson's Disease (PD) is one of the most common neurodegenerative disorders that primarily affects the motor system of the human body [14,20]. PD typically has a stealthy onset and is often clinically diagnosed in the mid to late stages, usually missing the optimal treatment window [16]. Therefore, an early and precise diagnosis of PD is crucial for timely therapeutic intervention [17]. Positron

† These authors contributed equally to this work.

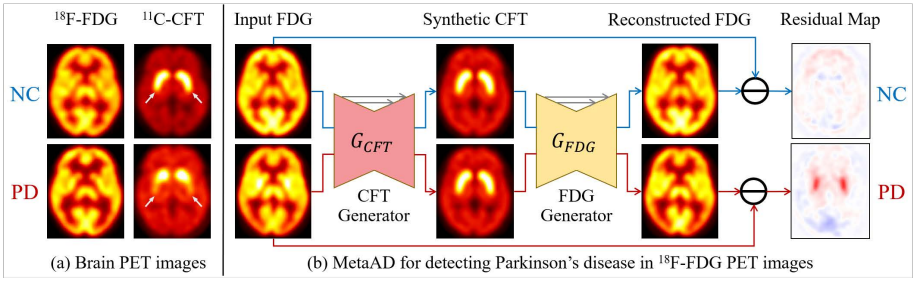

Fig. 1. (a) ^{11}C-CFT PET can reveal the differences between Parkinson's Disease (PD) and normal control (NC) while ^{18}F-FDG PET shows minimal visual differences. (b) The proposed MetaAD can highlight metabolic anomalies of PDs in FDG images. Red and blue regions denote abnormal areas of higher and lower metabolism, respectively.

Emission Tomography (PET) has emerged as a superior imaging modality in diagnosing neurological brain disorders [5]. The dopamine transporter (DAT) imaging such as ^{11}C-CFT PET has been utilized as a standard practice for discerning abnormal metabolisms for PD patients [26]. As shown in Fig. **??**(a), a ^{11}C-CFT PET scan can reveal functional alterations of dopaminergic neurons in the caudate and putamen regions [10]. Although ^{11}C-CFT PET has demonstrated significant superiority in diagnosing PD, most hospitals have to use the more generic ^{18}F-fluorodeoxyglucose (^{18}F-FDG) PET for PD diagnosis. Distinguishing PD patients from normal controls (NCs) in FDG images poses a challenge even for senior clinicians due to minimal visual differences [19]. It also inherently curtails the performance of deep learning-based computer-aided diagnosis (CAD) systems in diagnosing PD in FDG images [25].

An instinctive solution to the problem above would be to visually highlight significant areas of metabolic anomalies in FDG images, which can enhance the capability and interpretability of CADs without architecture modifications. Unsupervised anomaly detection (UAD) [4] emerges as a priority option because it can construct residual maps for abnormal samples to visually demonstrate their differences from normal samples. A typical UAD method first learns the reconstruction of normal images and then detects potential anomalies by evaluating the pixel difference between the input and reconstructed images. The underlying assumption is that a model solely trained on normal data will consistently reconstruct normal patterns regardless of the anomalies from the inputs. Autoencoders (AEs) [6, 23] or Generative Adversarial Networks (GANs) [1, 22] are usually employed to learn a compact latent space that represents the normal data distribution exclusively. However, optimizing the latent space is notoriously challenging, primarily due to the inability to intuitively observe what it has encoded. Some UAD methods utilize cyclic modality translation for image reconstruction [3, 15], which offers an intermediate image to visually represent normal characteristics in another modality. Nevertheless, these methods neces-

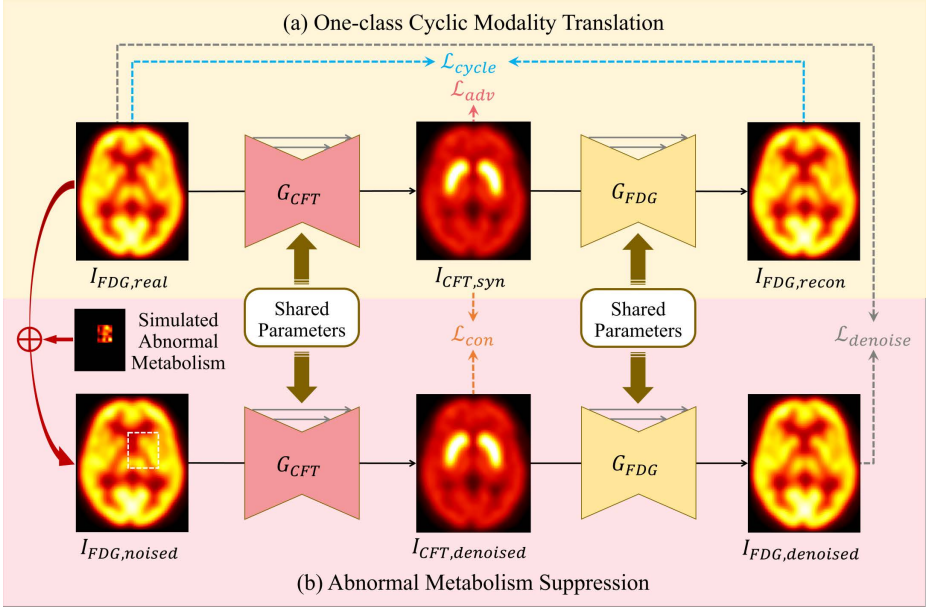

Fig. 2. The proposed MetaAD adopts a dual-path training scheme including (a) One-class Cyclic Modality Translation and (b) Abnormal Metabolism Suppression.

sitate paired data in training, and often excel in cross-modality mapping rather than accurately modeling tissue-specific normal features.

To address the issues above, we propose a **Meta**bolism-aware **A**nomaly **D**etection (MetaAD) framework to visually indicate abnormal metabolism cues of PD in ^{18}F-FDG PET scans. MetaAD consists of two generators as shown in Fig. 1(b). The CFT Generator acts as the encoder, embedding the input FDG image into the synthetic CFT image space that only represents healthy metabolic characteristics. The FDG Generator plays the role of the decoder, reconstructing the most similar normal FDG image from the distribution of synthetic CFT images. The intensity differences between the input and reconstructed FDG images result in a residual map, which highlights the areas of metabolic anomalies.

MetaAD adopts a dual-path training scheme as illustrated in Fig. 2. The main path **One-class Cyclic Modality Translation** prompts the generators to construct an explicit normal data distribution by cross-modality mapping. The parallel auxiliary path **Abnormal Metabolism Suppression** leverages the abnormal metabolism simulation mechanism to enhance the generators' ability of healthy metabolism modeling. The experiments demonstrate that MetaAD outperforms other UAD methods in detecting metabolic anomalies of PD, making it an effective and explainable tool for decision-making. Moreover, MetaAD can enhance the performance and interpretability of supervised CAD algorithms by simply incorporating the residual maps as additional inputs.

2 Method

As demonstrated in Fig. 2, MetaAD adopts a dual-path training scheme toward metabolism-aware learning. One-class Cyclic Modality Translation is the primary path that learns an explicit normal data distribution of CFT images and reconstructs normal FDG images via cross-modality translation. Abnormal Metabolism Suppression serves as an auxiliary path that reinforces MetaAD's ability to memorize healthy metabolic characteristics.

2.1 One-class Cyclic Modality Translation

Given the difficulty of acquiring paired FDG and CFT images for NC subjects in real clinical scenarios, we adopt the idea of CycleGAN [27] to train MetaAD on the unpaired dataset. As shown in Fig. 2(a), the CFT Generator G_{CFT} inputs a real FDG image $I_{FDG,real}$ to predict a synthetic CFT image $I_{CFT,syn}$ characterized by healthy metabolism, while the FDG Generator G_{FDG} outputs the reconstructed FDG image $I_{FDG,recon}$ via a reversed modality mapping from $I_{CFT,syn}$. All the PET images are 3D volumes with the same shape $H \times W \times D$. Two generators G_{CFT} and G_{FDG} adopt the same 3D U-Net architectures [21]. A voxel-wise ℓ_1 loss is implemented as the cycle-consistency loss $\mathcal{L}_{cycle}$ to reduce the metabolism difference between $I_{FDG,real}$ and $I_{FDG,recon}$:

$$\mathcal{L}_{cycle} = \mathbb{E}_{I_{FDG,real}, I_{FDG,recon}} \left[\| I_{FDG,real} - I_{FDG,recon} \|_{\ell_1} \right]. \tag{1}$$

To ensure that the intermediate CFT images capture healthy metabolic features, a 3D fully-convolutional PatchGAN discriminator D_{CFT} is employed to distinguish the real CFT images from the synthetic ones, thus forcing the synthetic metabolism of CFT images to match the real data distribution in an adversarial setting. The *hinge* version of the standard adversarial loss $\mathcal{L}_{adv}$ is used as the objective to optimize G_{CFT} and D_{CFT}.

In addition to training the forward flow of cyclic modality translation above, the same training settings are also implemented in the reversed cyclic modality translation flow, *i.e.*, CFT $\rightarrow$ FDG $\rightarrow$ CFT, thus enhancing the generators' ability of cross-modality translation as well as healthy metabolism modeling.

2.2 Abnormal Metabolism Suppression

MetaAD is theoretically expected to reconstruct normal FDG images only, but it sometimes fails to reconstruct healthy metabolic patterns for PD subjects via cyclic modality translation. The underlying reason lies in the training objectives of One-class Cyclic Modality Translation where the optimizations of cross-modality translation and healthy metabolism modeling are entangled. Thus, Abnormal Metabolism Suppression, an auxiliary but indispensable training path, is designed to facilitate metabolism-aware learning in training MetaAD.

The core idea of Abnormal Metabolism Suppression is to increase the difficulty of cyclic modality translation by simulating metabolic anomalies for the

input images, thereby forcing the models to memorize normal metabolic patterns. For abnormal metabolism simulation, we employ Poisson noises based on the clinical prior that Poisson noise is the dominant source of noises in PET imaging [24]. Specifically, we increase the unpredictability of Poisson noises by implementing the following three steps, thus preventing the models from easily grasping the anomalous patterns. Firstly, we randomly select a volumetric patch within the input image, preparing to fill it with the generated noise. Secondly, inspired by the observation that training with lower resolution noise leads to better anomaly detection than naive pixel-wise noise [12], we generate a coarse noise map by downsampling the selected patch and filling it with Poisson noise. Thirdly, we perturb the coarse noise map through cyclic shifting of matrix elements, upsample it to the original patch size, and add it to the selected location.

The abnormal metabolism simulation mechanism above cannot be directly applied to One-class Cyclic Modality Translation, thereby preventing the models from only recognizing abnormal patterns rather than normal ones. Instead, we build a parallel training flow for Abnormal Metabolism Suppression as illustrated in Fig. 2(b). The simulated abnormal metabolism is added to the real FDG image $I_{FDG,real}$ to formulate the input $I_{FDG,noised}$. The CFT Generator G_{CFT} learns to restore a denoised CFT image $I_{CFT,denoised}$ with complete healthy metabolism from $I_{FDG,noised}$. A voxel-wise ℓ_1 loss is employed as the consistency loss $\mathcal{L}_{con}$ to encourage the metabolism coherence between $I_{CFT,denoised}$ and $I_{CFT,syn}$ from One-class Cyclic Modality Translation:

$$\mathcal{L}_{con} = \mathbb{E}_{I_{CFT,syn},I_{CFT,denoised}} \left[\| I_{CFT,syn} - I_{CFT,denoised} \|_{\ell_1} \right]. \tag{2}$$

The FDG Generator then converts $I_{CFT,denoised}$ to the denoised FDG image $I_{FDG,denoised}$. Directly imposing a consistency constraint between $I_{FDG,denoised}$ and $I_{FDG,recon}$ from One-class Cyclic Modality Translation could lead to training instability. Considering that $I_{FDG,recon}$ is optimized toward $I_{FDG,real}$, we apply a voxel-wise ℓ_1 loss as the denoising loss $\mathcal{L}_{denoised}$ between $I_{FDG,denoised}$ and $I_{FDG,real}$ as the approximation of its consistency constraint with $I_{FDG,recon}$.

Similar to One-class Cyclic Modality Translation, the training settings above are also implemented to the reversed cyclic modality translation flow. The total objective $\mathcal{L}_{total}$ for MetaAD can be expressed by combining all losses above:

$$\mathcal{L}_{total} = \lambda_{cycle}\mathcal{L}_{cycle} + \lambda_{adv}\mathcal{L}_{adv} + \lambda_{con}\mathcal{L}_{con} + \lambda_{denoised}\mathcal{L}_{denoised}, \tag{3}$$

where we empirically set λ_{cycle} to 10, λ_{adv} and λ_{con} to 1, and $\lambda_{denoised}$ to 5.

2.3 Inference and Anomaly Scores

As described in Fig. 1(b), MetaAD produces a residual map where positive values (denoted in red) indicate abnormal metabolism increases while negative values (denoted in blue) represent decreases. While the visual differences are intuitively presented in the residual maps, it is non-trivial to define quantitative anomaly

scores for detecting PD metabolic anomalies. The maximum of the residual map, widely used in UAD methods, may not work well since the metabolic changes vary across different brain regions [11]. Therefore, we investigate the impact of the following four anomaly scores on PD diagnosis.

- **Highest Metabolic Anomaly (HMA)**. It measures the maximum of the residual map, which indicates the peak of abnormal metabolism increase.
- **Lowest Metabolic Anomaly (LMA)**. It measures the minimum of the residual map, which indicates the valley of abnormal metabolism decrease.
- **Abnormal Metabolism Range (AMR)**. It measures the difference between the maximum and minimum values in the residual map, which indicates the range of abnormal metabolic changes.
- **Averaged Metablism Change (AMC)**. It measures the mean value of the cycle-consistency loss $\mathcal{L}_{cycle}$ between the input and reconstructed images, which reflects the averaged change of metabolic anomalies.

3 Experimental Results

3.1 Dataset and Experimental Setup

Dataset We involve 274 PD patients and 330 NC subjects from Huashan Hospita. Each PD patient underwent a ^{18}F-FDG PET scan and a ^{11}C-CFT PET scan. For NC subjects, 154 subjects underwent a ^{18}F-FDG PET scan, 154 subjects underwent a ^{11}C-CFT PET scan, and 22 subjects underwent two PET imaging scans. Each PET scan is registered to standard MNI 152 space and cropped to $96 \times 80 \times 72$ in $2 \times 2 \times 2$ mm resolution.

Implementation Details We conduct 5-fold cross-validations on all the experiments using an NVIDIA A100 GPU with PyTorch [18]. To be specific, we first combine 274 PD FDG images and 154 NC FDG images that have no paired CFT scans. Then we randomly split them into five groups, each of which served as the testing set in turn with the remaining four groups as the training set. When training MetaAD, only the NC FDG images in the training set are used together with all 154 unpaired NC CFT images. The remaining 22 paired PET images of NC subjects are particularly used to evaluate the qualitative performance of MetaAD. We use the learning rate of 2×10^{-4}, batch size of 4, and Adam optimizer [13] to train MetaAD for $20k$ iterations.

3.2 Comparison with Other UAD Methods

We first compare MetaAD with other UAD architectures in visually detecting PD metabolic anomalies in FDG images. As shown in Fig. 3, AE and U-Net struggle to identify PD metabolic anomalies even though they can reconstruct NC FDG images well. Both CycleGAN and MetaAD succeed in detecting high-metabolism areas, but CycleGAN falls short in delineating low-metabolism areas as precisely

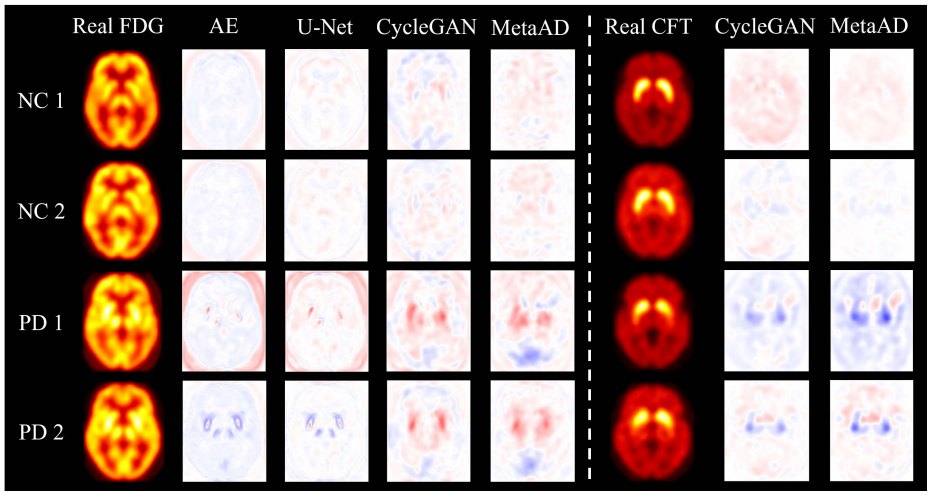

Fig. 3. Qualitative comparison between MetaAD and other methods. Red and blue in residual maps denote abnormal areas of higher and lower metabolism, respectively.

Table 1. Quantitative comparison of sensitivity based on different anomaly scores.

Method	HMA	LMA	AMR	AMC
AE [2]	$60.82_{\pm 7.17}$	$86.89_{\pm 5.04}$	$60.79_{\pm 7.04}$	$2.17_{\pm 2.15}$
U-Net [21]	$34.97_{\pm 7.19}$	$78.20_{\pm 6.22}$	$50.05_{\pm 7.41}$	$21.54_{\pm 6.11}$
CycleGAN [27]	$62.95_{\pm 7.23}$	$71.69_{\pm 6.61}$	$\mathbf{76.11_{\pm 6.12}}$	$50.07_{\pm 7.37}$
MetaAD (Ours)	$\mathbf{69.52_{\pm 7.08}}$	$\mathbf{91.44_{\pm 4.13}}$	$69.45_{\pm 6.61}$	$\mathbf{76.09_{\pm 6.20}}$

as MetaAD. Moreover, MetaAD outperforms CycleGAN in accurately identifying abnormal metabolism for real PD CFT images, indicating its superiority in modeling health metabolic patterns for both FDG and CFT modalities.

We also compare their quantitative performance based on four predefined anomaly scores. The sensitivity results are shown in Table 1 while other evaluation metrics are presented in *Supplementary Materials*. It is observed that MetaAD exhibits the best performance across almost all anomaly scores. Notably, MetaAD achieves significantly higher sensitivity than CycleGAN in terms of LMA, an outcome consistent with their qualitative comparison above.

3.3 Ablation Study

We conduct an ablation study to verify the effects of the proposed dual-path training scheme. Starting with One-class Cyclic Modality Translation only, we integrate each key component step-by-step and report the performance based on LMA in Table 2. First, directly adding simulated metabolic anomalies to One-class Cyclic Modality Translation leads to a decline in performance. In contrast, the performance can be greatly improved if a parallel training path is implemented to tackle the simulated abnormal metabolism. Second, the consistency

Table 2. Ablation study of the key components: (a) Abnormal metabolism simulation (AMS), (b) parallel training path. (c) consistency loss $\mathcal{L}_{con}$, (d) Poisson noise.

Configuration				LMA			
AMS	Parallel	$\mathcal{L}_{con}$	Noise	Accuracy	Sensitivity	Specificity	AUC
×	×	×	×	$73.66_{\pm 5.58}$	$71.69_{\pm 6.61}$	$77.39_{\pm 8.97}$	$79.65_{\pm 5.75}$
✓	×	×	Poisson	$70.70_{\pm 5.64}$	$71.72_{\pm 6.69}$	$68.23_{\pm 9.85}$	$75.34_{\pm 6.21}$
✓	✓	×	Poisson	$77.87_{\pm 5.03}$	$82.65_{\pm 5.65}$	$68.66_{\pm 10.02}$	$81.25_{\pm 5.73}$
✓	✓	✓	Gaussian	$76.66_{\pm 5.03}$	$73.77_{\pm 6.26}$	$\mathbf{81.46_{\pm 8.33}}$	$80.31_{\pm 6.02}$
✓	✓	✓	Poisson	$\mathbf{83.82_{\pm 4.48}}$	$\mathbf{91.44_{\pm 4.13}}$	$67.92_{\pm 10.09}$	$\mathbf{83.97_{\pm 5.54}}$

loss between two intermediate synthetic CFT images can further enhance the performance as it facilitates the information flow between training paths. In addition, applying Gaussian noise to simulate abnormal metabolism for training MetaAD is suboptimal, which suggests that the utilization of Poisson noise aligns more accurately with real-world scenarios.

Table 3. MetaAD can effectively improve the classification performance of various supervised classification models in diagnosing PD in ^{18}F-FDG PET images.

Classifier	MetaAD	Accuracy	Sensitivity	Specificity	F1-Score	AUC
ResNet [7]	×	$79.37_{\pm 3.31}$	$80.64_{\pm 11.22}$	$77.39_{\pm 17.61}$	$83.34_{\pm 3.48}$	$90.44_{\pm 6.41}$
	✓	$\mathbf{86.52_{\pm 3.73}}$	$\mathbf{91.58_{\pm 5.31}}$	$\mathbf{77.42_{\pm 16.20}}$	$\mathbf{89.75_{\pm 2.42}}$	$\mathbf{94.20_{\pm 2.43}}$
DenseNet [9]	×	$81.34_{\pm 6.24}$	$79.44_{\pm 17.58}$	$\mathbf{84.59_{\pm 17.94}}$	$83.79_{\pm 7.53}$	$94.13_{\pm 2.61}$
	✓	$\mathbf{87.08_{\pm 4.01}}$	$\mathbf{88.69_{\pm 3.74}}$	$84.14_{\pm 8.47}$	$\mathbf{89.85_{\pm 2.95}}$	$\mathbf{94.54_{\pm 1.80}}$
SEResNet [8]	×	$81.04_{\pm 4.28}$	$84.13_{\pm 6.30}$	$75.64_{\pm 9.12}$	$85.12_{\pm 3.54}$	$89.95_{\pm 2.92}$
	✓	$\mathbf{89.32_{\pm 1.45}}$	$\mathbf{92.21_{\pm 1.14}}$	$\mathbf{84.08_{\pm 2.63}}$	$\mathbf{91.78_{\pm 1.19}}$	$\mathbf{93.89_{\pm 1.28}}$

3.4 Effectiveness in Assisting Supervised Learning

To validate the effectiveness of MetaAD in assisting supervised learning algorithms for PD diagnosis in FDG images, we conduct 5-fold cross-validations on the PD/NC classification performance of three different classifiers (*i.e.*, ResNet [7], DenseNet [9], and SEResNet [8]) using the produced residual maps. Specifically, each FDG image is concatenated with its residual map to establish the input. As shown in Table 3, all the classifiers achieve significant improvements using residual maps as additional inputs. This illustrates that MetaAD can effectively aid the supervised CAD systems in PD diagnosis and provide visual interpretations by directly highlighting abnormal metabolism regions in FDG images.

4 Conclusion and Discussion

In this paper, we propose MetaAD, a novel metabolism-aware anomaly detection framework, to visually highlight abnormal metabolism cues of PD in ^{18}F-FDG

PET scans. We design a dual-path training path where One-class Cyclic Modality Translation enables MetaAD to explicitly represent normal data distribution through cross-modality conversion, while Abnormal Metabolism Suppression prompts MetaAD to memorize normal metabolic patterns via the abnormal metabolism simulation mechanism. Comprehensive experiments demonstrate the visual interpretability and anomaly detection superiority of MetaAD, as well as its effectiveness in assisting supervised CAD methods in PD diagnosis. Still, MetaAD falls short in differentiating PD from other atypical Parkinsonian syndromes, which would be targeted in the future.

Acknowledgments. This research was partially supported by National Natural Science Foundation of China (82394432, 82394434, 82272039, 82021002, 81971641) and STI 2030-Major Projects (2022ZD0211600).

Disclosure of Interests. The authors have no competing interests to declare that are relevant to the content of this article.

References

1. Akcay, S., Atapour-Abarghouei, A., Breckon, T.P.: Ganomaly: Semi-supervised anomaly detection via adversarial training. In: Computer Vision–ACCV 2018: 14th Asian Conference on Computer Vision, Perth, Australia, December 2–6, 2018, Revised Selected Papers, Part III 14. pp. 622–637. Springer (2019)
2. Baur, C., Denner, S., Wiestler, B., Navab, N., Albarqouni, S.: Autoencoders for unsupervised anomaly segmentation in brain mr images: a comparative study. Medical Image Analysis **69**, 101952 (2021)
3. Baur, C., Graf, R., Wiestler, B., Albarqouni, S., Navab, N.: Steganomaly: Inhibiting cyclegan steganography for unsupervised anomaly detection in brain mri. In: International Conference on Medical Image Computing and Computer-Assisted Intervention. pp. 718–727. Springer (2020)
4. Fernando, T., Gammulle, H., Denman, S., Sridharan, S., Fookes, C.: Deep learning for medical anomaly detection–a survey. ACM Computing Surveys (CSUR) **54**(7), 1–37 (2021)
5. Golan, H., Volkov, O., Shalom, E.: Nuclear imaging in parkinson's disease: The past, the present, and the future. Journal of the Neurological Sciences **436**, 120220 (2022)
6. Gong, D., Liu, L., Le, V., Saha, B., Mansour, M.R., Venkatesh, S., Hengel, A.v.d.: Memorizing normality to detect anomaly: Memory-augmented deep autoencoder for unsupervised anomaly detection. In: Proceedings of the IEEE/CVF International Conference on Computer Vision. pp. 1705–1714 (2019)
7. He, K., Zhang, X., Ren, S., Sun, J.: Deep residual learning for image recognition. In: Proceedings of the IEEE conference on computer vision and pattern recognition. pp. 770–778 (2016)
8. Hu, J., Shen, L., Albanie, S., Sun, G., Wu, E.: Squeeze-and-excitation networks (2019)
9. Huang, G., Liu, Z., Van Der Maaten, L., Weinberger, K.Q.: Densely connected convolutional networks. In: Proceedings of the IEEE conference on computer vision and pattern recognition. pp. 4700–4708 (2017)

10. Ishibashi, K., Oda, K., Ishiwata, K., Ishii, K.: Comparison of dopamine transporter decline in a patient with parkinson's disease and normal aging effect. Journal of the neurological sciences **339**(1-2), 207–209 (2014)
11. Jiang, C., Ge, J., Shi, X., WU, J., Wang, J., WU, P., Zhang, X., Zuo, C., Guan, Y.: Characteristics of cerebral glucose metabolism on 18f-fdg pet imaging in patients with parkinson's disease. Chinese Journal of Nuclear Medicine and Molecular Imaging pp. 193–197 (2017)
12. Kascenas, A., Sanchez, P., Schrempf, P., Wang, C., Clackett, W., Mikhael, S.S., Voisey, J.P., Goatman, K., Weir, A., Pugeault, N., et al.: The role of noise in denoising models for anomaly detection in medical images. Medical Image Analysis **90**, 102963 (2023)
13. Kingma, D.P., Ba, J.: Adam: A method for stochastic optimization (2015)
14. Kish, S.J., Shannak, K., Hornykiewicz, O.: Uneven pattern of dopamine loss in the striatum of patients with idiopathic parkinson's disease. New England Journal of Medicine **318**(14), 876–880 (1988)
15. Liang, Z., Anthony, H., Wagner, F., Kamnitsas, K.: Modality cycles with masked conditional diffusion for unsupervised anomaly segmentation in mri. In: International Conference on Medical Image Computing and Computer-Assisted Intervention. pp. 168–181. Springer (2023)
16. Odekerken, V.J., van Laar, T., Staal, M.J., Mosch, A., Hoffmann, C.F., Nijssen, P.C., Beute, G.N., van Vugt, J.P., Lenders, M.W., Contarino, M.F., et al.: Subthalamic nucleus versus globus pallidus bilateral deep brain stimulation for advanced parkinson's disease (nstaps study): a randomised controlled trial. The Lancet Neurology **12**(1), 37–44 (2013)
17. Pagan, F.L.: Improving outcomes through early diagnosis of parkinson's disease. American Journal of Managed Care **18**(7), S176 (2012)
18. Paszke, A., Gross, S., Massa, F., Lerer, A., Bradbury, J., Chanan, G., Killeen, T., Lin, Z., Gimelshein, N., Antiga, L., et al.: Pytorch: An imperative style, high-performance deep learning library. Advances in neural information processing systems **32** (2019)
19. Peralta, C., Strafella, A.P., van Eimeren, T., Ceravolo, R., Seppi, K., Kaasinen, V., Arena, J.E., Lehericy, S., Group, I.P.M.D.S.N.S.: Pragmatic approach on neuroimaging techniques for the differential diagnosis of parkinsonisms. Movement Disorders Clinical Practice **9**(1), 6–19 (2022)
20. Pringsheim, T., Jette, N., Frolkis, A., Steeves, T.D.: The prevalence of parkinson's disease: a systematic review and meta-analysis. Movement disorders **29**(13), 1583–1590 (2014)
21. Ronneberger, O., Fischer, P., Brox, T.: U-net: Convolutional networks for biomedical image segmentation. In: Medical Image Computing and Computer-Assisted Intervention–MICCAI 2015: 18th International Conference, Munich, Germany, October 5-9, 2015, Proceedings, Part III 18. pp. 234–241. Springer (2015)
22. Schlegl, T., Seeböck, P., Waldstein, S.M., Langs, G., Schmidt-Erfurth, U.: f-anogan: Fast unsupervised anomaly detection with generative adversarial networks. Medical image analysis **54**, 30–44 (2019)
23. Shvetsova, N., Bakker, B., Fedulova, I., Schulz, H., Dylov, D.V.: Anomaly detection in medical imaging with deep perceptual autoencoders. IEEE Access **9**, 118571–118583 (2021)
24. Song, T.A., Yang, F., Dutta, J.: Noise2void: unsupervised denoising of pet images. Physics in Medicine & Biology **66**(21), 214002 (2021)

25. Wang, J., Xue, L., Jiang, J., Liu, F., Wu, P., Lu, J., Zhang, H., Bao, W., Xu, Q., Ju, Z., et al.: Diagnostic performance of artificial intelligence-assisted pet imaging for parkinson's disease: a systematic review and meta-analysis. NPJ Digital Medicine **7**(1), 17 (2024)
26. Zhao, Y., Wu, P., Wu, J., Brendel, M., Lu, J., Ge, J., Tang, C., Hong, J., Xu, Q., Liu, F., et al.: Decoding the dopamine transporter imaging for the differential diagnosis of parkinsonism using deep learning. European journal of nuclear medicine and molecular imaging **49**(8), 2798–2811 (2022)
27. Zhu, J.Y., Park, T., Isola, P., Efros, A.A.: Unpaired image-to-image translation using cycle-consistent adversarial networks. In: Proceedings of the IEEE international conference on computer vision. pp. 2223–2232 (2017)